

文章编号:1000-0615(2005)02-0238-08

A numerical model for predicting the fishing operation status of tuna longlines

WAN Rong, CUI Jiang-hao, SONG Xie-fa, TANG Yan-li, ZHAO Fen-fang, HUANG Liu-yi
(Fisheries College, Ocean University of China, Qingdao 266003, China)

Abstract: In this paper, ropes are modeled as an infinitely flexible, straight rope element, and then the whole longline is able to be regarded as an assembling of the rope elements connecting each other at their ends by a frictionless hinge. A group of nonlinear basic simultaneous equations describing the equilibrium state of longlines are deduced, based on a finite element formulation. Newton-Raphson method is employed to get the numerical solution due to the non-linearity. Further, the loading and shape iterative procedure are used to model the coupling relationship between the longline shape and hydrodynamic forces. The results suggested that this method has excellent global convergence and good accuracy for predicting the tension and shape of tuna longlines during fishing operation.

Key words: finite element analysis; tuna; long line; tension and shape

CLC number: S972

Document code: A

1 Introduction

There are concerns about the distant water fisheries with the decline of the marine fisheries resources offshore and inshore due to over-fishing. The tuna fishery is one of the hot topics and becomes an important part of the world pelagic fisheries since tunas and tuna-like species, caught mainly by distant water longlines and purse seines, have high meat quality and remarkable economy value, especially in Japanese sasimi market. Tuna stocks have been found in the Pacific, Atlantic, and Indian Oceans and the total yield of its four main species has been maintained at the level of about 4 million tons a year in the recent years^[1]. Tuna fishery of China started in 1987 and achieved remarkable progress. By the year of 1999, the total fishing production of tuna had exceeded 20 000 tons and more than 200 longliners are in operation in the three oceans of the world^[2].

Longline, as a type of the efficient conventional fishing gear, has been widely used in commercial tuna fishery because of the simplicity in its design, construction and operation and of the low investment cost as well as the low energy consumption. A tuna longline consists of mainline, branch-lines, hooks,

buoy lines and buoys. In order to capture fish with satisfaction, the hooks have to reach the water depth where tunas live or are swimming during fishing operation by adjusting the gear configuration and correctly setting the gear. Therefore, it is very important to develop a tool of predicting the depth that the hooks possibly reach during fishing operation.

So far, the tension and shape of longlines have not been solved theoretically because of its complexity. Generally, the setting depth of the hooks is estimated by assuming that the distance of mainline between the two neighboring buoys maintains unchangeable and that the mainline forms a catenary during operation^[3-6]. In addition, the prediction of longline behavior can also be done by flume tank testing and field experiment^[7,8].

In this paper, the longline is considered as a flexible rope system and a method based on a finite element formulation is used to analyze the tension and shape of the longline. The aim of this study is to find a more economical and practical tool to replace the model test and field experiment, which are laborious, time-consuming and expensive, for optimizing longline design and construction.

Received date: 2003-07-14

Foundation item: Shandong Province Science Encouragement Foundation for Midfile; Youth Scientist and Project-sponsored by SRF for ROCS, SEM; the SRFDP of China under grant No. 20040423007

Brief introduction of the author: Wan Rong (1963 -), male, born in Wenling City, Zhejiang Province, professor, Ph. D, interested in mechanics of fishing gears and numerical simulation on mariculture engineering. E-mail: rongwan@ouc.edu.cn

2 Mathematical model

2.1 Modeling of the rope

The longline is a regular fishing gear that is mainly composed of ropes and hooks. The ropes can be modeled by a series of straight discrete rope elements (Fig. 1, hereafter referred to as rope element or element)^[9-12], connected each other at their ends by non-frictional hinges. If each end of the element is called as a node, the whole structure can be regarded as an assembling of the elements articulated at their nodes.

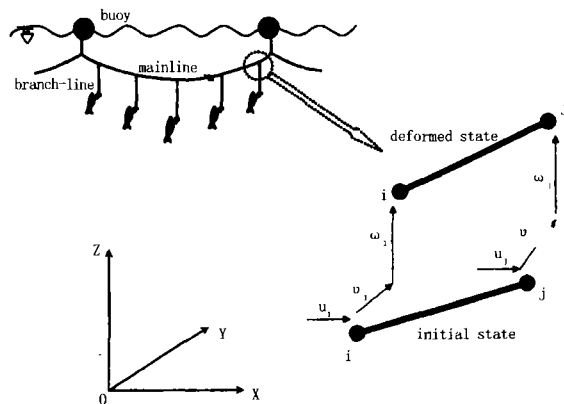


Fig.1 Movement of a straight rope element
 X , Y and Z are global coordinates system. u , v and ω denote the nodal displacements of the element in the direction of the X , Y and Z -axes, respectively. The subscripts i and j indicate the two ends of the element

2.2 Basic hypotheses

In order to simplify the mathematical model, the following assumptions for the physical characteristic of the rope should be made^[9,10]:

(1) The tension only acts in the direction of the axis of element and keeps constant across the entire cross-section and along the element length;

(2) The rope is completely flexible and easily bent without resistance;

(3) The rope is elastic and isotropic, and the relationship between the tension and strain follows Hooke's law;

(4) The relative displacements are equal for all points on the cross-section of the element, and the cross-sectional area remains constant during deformation.

2.3 Basic equations

When a longline is set in a uniform current, the

rope elements comprising it will incur significant relative displacement from any initial state to a deformed state (Fig. 1). According to the above hypotheses, the total potential energy Π for the discrete system can be expressed as^[11-13]

$$\Pi = - \sum_{i=1}^n F_i D_i + \sum_{g=1}^m T_g \{ L_g(D_i) - L_{g0} \} - \sum_{g=1}^m \frac{L_{g0}}{2EA_g} T_g^2 \quad (1)$$

where F_i is the equivalent nodal loading on the i -th node, D_i is the displacement of the i -th node, T_g is the axial force of the g -th element, L_{g0} is the initial length of the g -th element, L_g is the length of the g -th element after deformation, A_g is cross-section area of the g -th element, E is the Young's modulus of the material, f is the nodal degree of freedom, and m is the total number of the element. The term in $\{ L_g(D_i) - L_{g0} \}$ Equation (1) represents the elastic elongation of the g -th element due to tensile forces or finite displacements of the elements during large deformation, and can be explicitly written as

$$L_g(D_i) - L_{g0} = \sqrt{X(u)^2 + Y(v)^2 + Z(w)^2} - \sqrt{X_0^2 + Y_0^2 + Z_0^2} \quad (2)$$

where

$$X_0 = X_j - X_i, Y_0 = Y_j - Y_i, Z_0 = Z_j - Z_i \quad (3)$$

$$\left. \begin{aligned} X(u) &= (X_j - X_i) + (u_j - u_i) \\ Y(v) &= (Y_j - Y_i) + (v_j - v_i) \\ Z(w) &= (Z_j - Z_i) + (w_j - w_i) \end{aligned} \right\} \quad (4)$$

and X , Y and Z are the nodal coordinates of the element in the direction of the X , Y and Z -axes in a global frame of reference. The X and Z -axes point to the current and water depth respectively, the Y -axis is vertical to both the X and Z -axes. As shown in Fig.1, the variables u , v and ω denote the nodal displacements of the element in the direction of the X , Y and Z -axes, respectively. The subscripts i and j indicate the two ends of the element. Equations (2-4) describe the strain-displacement relationship for the elements.

For the purpose of determining the equilibrium state of the instable rope system, the principle of minimum potential energy is applied. According to the principle, the total potential energy becomes an absolute minimum when the system is under equilibrium condition, i.e., $\partial \Pi / \partial D_i = 0$ and $\partial \Pi / \partial T_g = 0$. Then the following basic equations for this system can be obtained:

$$\begin{bmatrix} \frac{\partial L_1}{\partial D_1} & \dots & \dots & \dots & \frac{\partial L_m}{\partial D_1} \\ \vdots & & & & \vdots \\ \frac{\partial L_1}{\partial D_j} & \dots & \dots & \dots & \frac{\partial L_m}{\partial D_j} \end{bmatrix} \begin{bmatrix} T_1 \\ \vdots \\ T_m \end{bmatrix} = \begin{bmatrix} F_1 \\ \vdots \\ F_j \end{bmatrix} \quad (5)$$

$$\{L_g(D_i) - L_{g0}\} - \frac{L_{g0}}{EA_g} T_g = 0, g = 1, 2, \dots, m. \quad (6)$$

The elements in the coefficient matrix in Equation(5) denote the direction cosines of the g -th element after deformation with respect to the X , Y and Z -axis, respectively. Equation (6) gives the relationship between element tension and nodal displacement. Consequently, the nonlinear Equations (5, 6) clearly constitute the basic simultaneous equations for $(f + m)$ degrees of freedom with unknowns of nodal displacement D_i and element tension T_g for the static response of the longlines.

2.4 Shape-dependent hydrodynamic loading

In Equation(5), the external force (F) acting on the elements includes those resulting from gravity (weight and buoyancy), hydrodynamic loading and other kinds of external action. Since the hydrodynamic loading containing lift (R_L), drag (R_D) and transverse force (R_H) are shape-dependent, it is difficult to be calculated theoretically. When neglecting the hydrodynamic interaction and interference between the elements, that is, it seemed as if the elements in the whole structure system are independent of each other in a current field, the hydrodynamic forces acting on each rope element can be estimated by the following formulas^[14].

$$R_D = \frac{1}{2} \rho C_D dLV^2 \quad (7)$$

$$R_L = \frac{1}{2} \rho C_L dLV^2 \quad (8)$$

$$R_H = \frac{1}{2} \rho C_H dLV^2 \quad (9)$$

where R_D , R_L and R_H are the hydrodynamic drag, lift and transverse force acting on the elements, respectively. d is the cross-sectional diameter of the element, L is the element length, V is the relative velocity of the flow, and ρ is the fluid density. The hydrodynamic lift, drag and transverse force coefficients (C_L , C_D and C_H) for ropes are given by the Miyazaki model^[14].

$$C_D = C_{D0}(1 - \sin^2\theta \cos^2\delta) \quad (10)$$

$$C_L = C_{D0} \sin\theta \cos^2\theta \cos^2\delta \quad (11)$$

$$C_H = C_{D0} \frac{\sin\theta \sin^2\delta \cos\delta}{\sqrt{1 - \cos^2\theta \cos^2\delta}} \quad (12)$$

where C_{D0} is the coefficient of drag when the axis of the element is vertical to the current, δ is the deflected angle, and θ is the inclined angle of the element, as shown in Fig. 2. The hydrodynamic force coefficients usually depend on Reynolds number Re calculated with the twine diameter. Because the Re is within the range of 6×10^2 to 2×10^3 in this study, let the C_{D0} equal 1.3^[14].

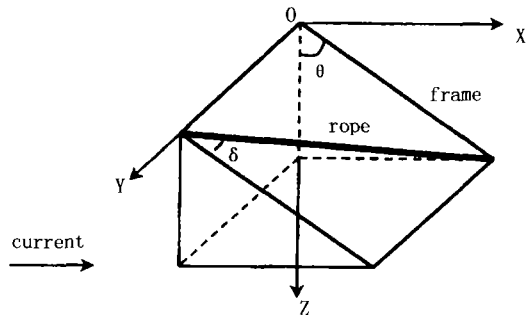


Fig. 2 Schematic diagram of rope position relative to the current
 δ is the deflected angle, and
 θ is the inclination angle of the element

2.5 Solution

Since the simultaneous Equations (5, 6) are highly nonlinear, Newton-Raphson method^[11-13] was adopted to find the numerical solution of the problem in this paper. As a result, the linearized basic equation can be expressed as:

$$\left. \begin{aligned} \sum_{i=1}^f \frac{\partial f_1}{\partial D_i} \Delta D_i + \sum_{g=1}^m \frac{\partial f_1}{\partial T_g} \Delta T_g + f_1(D_i^r, T_g^r) &= 0 \\ \sum_{i=1}^f \frac{\partial f_2}{\partial D_i} \Delta D_i + \sum_{g=1}^m \frac{\partial f_2}{\partial T_g} \Delta T_g + f_2(D_i^r, T_g^r) &= 0 \\ \dots\dots\dots \\ \sum_{i=1}^f \frac{\partial f_{f+m}}{\partial D_i} \Delta D_i + \sum_{g=1}^m \frac{\partial f_{f+m}}{\partial T_g} \Delta T_g + f_{f+m}(D_i^r, T_g^r) &= 0 \end{aligned} \right\} \quad (13)$$

where the (D_i^r, T_g^r) and $(\Delta D_i^r, \Delta T_g^r)$ denote the solution and the correction obtained in the r -th step of the iteration. Therefore, it is certain that the solution in the $(r + 1)$ -th step of the iteration can be written as $(D_i^r + \Delta D_i^r, T_g^r + \Delta T_g^r)$. Transforming Equations 13 into a simpler matrix form, then we have

$$\begin{bmatrix} N_{11} & N_{12} \\ N_{21} & N_{22} \end{bmatrix} \begin{Bmatrix} \Delta D_i^r \\ \Delta T_g^r \end{Bmatrix} =$$

$$\left\{ \begin{array}{l} F - \sum_{\mu=1}^m \frac{\partial L_{\mu}}{\partial D_i} T_{\mu} \\ \sum_{\mu=1}^m \frac{L_{\mu 0}}{EA_{\mu}} T_{\mu} + \{ L_{\mu 0} - L_{\mu}(D_i) \} \end{array} \right\}^T \quad (14)$$

whereby the submatrix $[N_{11}(D_i, T_{\mu})]$ corresponds to the geometrical stiffness matrix; $[N_{12}(D_i, T_{\mu})]$ is the equilibrium matrix of the system after deformation. $[N_{22}] = \text{diag}(-L_{\mu 0}/EA_{\mu})$; and $[N_{21}]$ is the compatibility matrix related to $[N_{12}]$ by^[9-11]

$$[N_{21}] = [N_{12}]^T \quad (15)$$

The total stiffness coefficient matrix is a function of the tension and nodal coordinates of elements in the global system after deformation. Superscript T of Equation(15) denotes the transposition of the matrix. So, following the computing flowchart shown in Fig. 3, a desired solution can be converged by the combination of the shape iteration cycle with the loading iterations procedure.

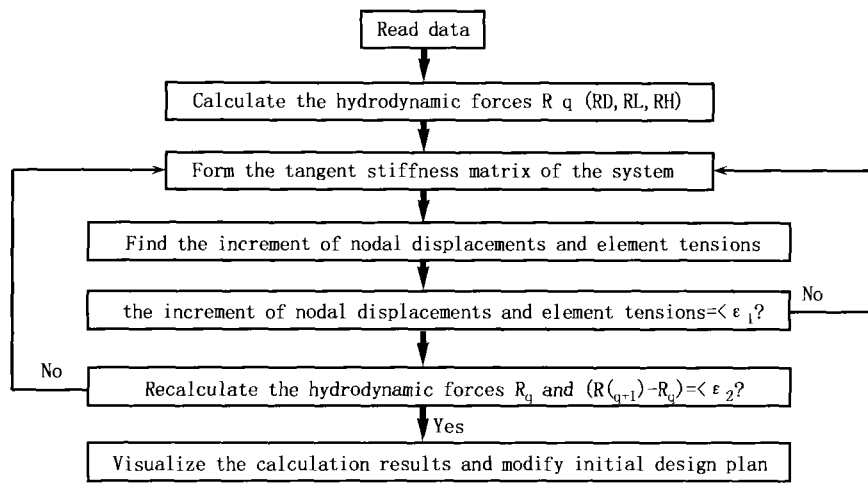


Fig.3 Computer support in the design of long line

2.6 Numerical example and model test

To validate the numerical model presented above, as an illustrative example, the fishing operation status of a simplified tuna longline model set in a uniform current was analyzed, and the corresponding model test was conducted in a flume tank at Tokyo University of Fisheries. The layout of the experimental system for measuring the shape of the simplified longline model is shown in Fig.4. The model was placed in a uniform current and the ends of the mainline were fixed to the supporting bars at a shortening rate of 0.95 for the mainline in the experiment. Because of the size limit of the water tank, the model had only three branch-lines (generally there are 5 to 16 branch-lines between the neighboring buoys in commercial tuna longline fishery^[3-5]). Model ropes were made of polypropylene, and the length of mainline and branch-line were 2.4m and 0.6m, respectively. In order to avoid over-blowing downstream and to facilitate the observation of the working shape of the ropes, a line-shaped lead was wrapped inside the ropes, and three

spherical sinkers with 27g each in water (Fig.4, large solid circles) were attached to the free end of the branch-lines for modeling the hooks, respectively. The ropes are 6mm in diameter and $75 \text{ g} \cdot \text{m}^{-1}$ in water.

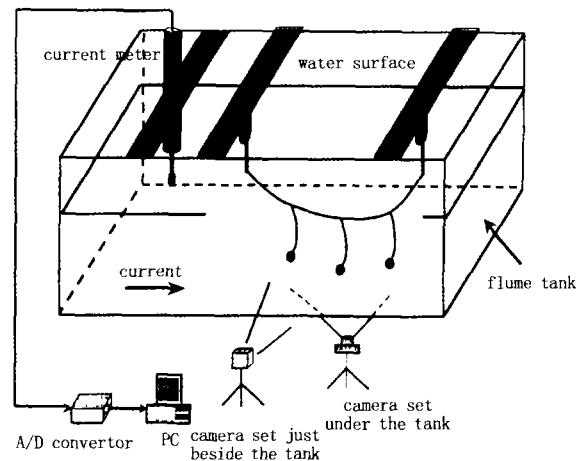


Fig.4 The layout of the experimental system for measuring the shapes of the simplified long-line model

As shown in Fig. 4, the velocity was measured by a propeller flow meter set in upstream. The equilibrium shape of the model longline was measured by using images taken simultaneously by two digital video cameras, set under and just beside the water tank respectively. The images were analyzed by "DIPP- MOTION 2D" digital image analysis software, producing a set of 3-D coordinates for all measured nodes. The errors due to the inadequacies in the optical system, such as the distortion by water refraction and the parallax by the difference in distance from objects to the center of camera lens, have been corrected^[12].

In this numerical example, the mainline was equally divided into 8 elements of 0.3 m and divided each branch-line into 3 elements of 0.2 m. As a result, there are 17 elements and 18 nodes in the whole system (Fig. 5, top-left). The dotted line is an initially assumed configuration of the simplified model for the nonlinear calculation, that is, the mainline was assumed to be an isosceles triangle and the branch-lines vertically direct down. In the top-left figure, the small solid circles express the virtual nodes of the elements, and the large solid circles indicate the spherical sinkers.

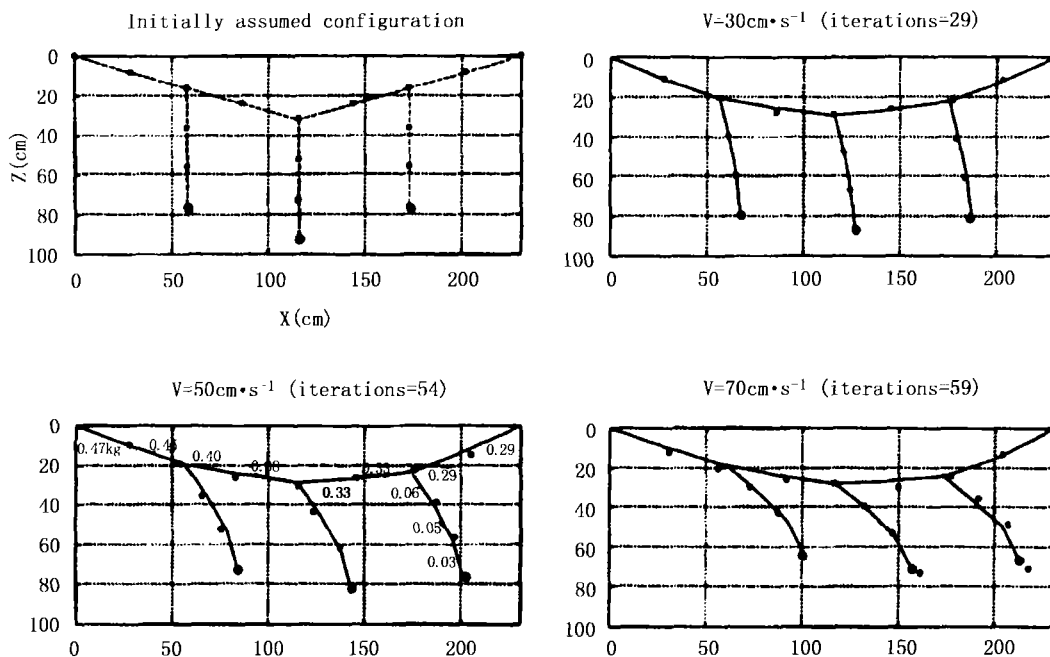


Fig. 5 Effect of current speed on the shape of the long-line model when placed parallel to the current

In addition, the horizontal distance of mainline between the two neighboring buoys almost remains constant during operation according to the experience from fishermen. So, it can be supposed that the two ends of the model longline are fixed in our experiment and numerical computation, that is, their displacements in X , Y and Z directions are zero.

3 Results

3.1 Status of the longline model when parallel to the current

The calculated shapes of the model longline and its measured values, when set parallel to a uniform current, are shown in Fig. 5. In this figure (except

the top-left), the solid lines express the calculated shapes when $V = 0.3, 0.5$ and $0.7 \text{ m} \cdot \text{s}^{-1}$, the small and large solid circles express the measured values of the virtual nodes of the elements and the spherical sinkers respectively. It is apparent that the theoretical and experimental values are in close agreement, although the calculated positions of the middle and the downstream-most branch-line are somewhat inaccurate under the high velocity of current. The model longline is skewed downstream, and it is different from the common thought that the mainline conforms to a standard catenary as a result of the hydrodynamic forces. The great variations of the shape of the model longline with the increasing of flow speed from $V =$

0.3 to $0.7 \text{ m} \cdot \text{s}^{-1}$ were well simulated. With the increase of the hydrodynamic forces acting on the ropes, the branch-lines were remarkably blown and the setting depth of the hooks evidently reduced by nearly 0.2m in the case of $V = 0.7 \text{ m} \cdot \text{s}^{-1}$ (Fig. 5, comparing top-right with low-right).

The values near each element (Fig. 5, left-low; unit: kg) indicate the tensions of the corresponding elements when $V = 0.5 \text{ m} \cdot \text{s}^{-1}$, as an illustrative example. The tension simulation result suggests that the tensile force of the element decrease gradually in the downstream direction and that the highest tension is on the upstream-most fixed end of mainline. The tension is much higher in the mainline than in the branch-lines.

3.2 Status of the long line model inclined to a current

Because longline operation is not always parallel to the current in tuna fishery, the validity of the proposed method, when aligned at an angle (α) relative to the current, has to be examined also. In contrast to configuration parallel to the current, it is clear that the model has a 3-D configuration in this situation (Fig. 6).

Fig. 6 demonstrates the effect of current speed on the shape of the model longline when $\alpha = 10^\circ$. Similar to the case parallel to current, the shape of the mainline formed a rough catenary. The shape of the

branch-lines greatly changed with increasing flow speed from $V = 0.3, 0.5$ to $0.7 \text{ m} \cdot \text{s}^{-1}$, that is, the setting depth of the hooks was remarkably getting shallower as a result of increasing current.

For the sake of convenience, the computations were started from a simple assumed shape in this case, i. e. mainline is an isosceles triangle and the branch-lines are upright, and the panel formed by the mainline and branch-lines is at an angle of 10° relative to the current (Fig. 6, top-left).

Further, the comparisons of the experimental data with the calculated results for $V = 0.5 \text{ m} \cdot \text{s}^{-1}$ and $\alpha = 10^\circ$ are shown in Fig. 7. The calculated results for the geometry (solid lines) are very close to the experimental values (solid circles). In the top view of the system (Fig. 7, low), it is demonstrated very well by the numerical model that the mainline curves slightly downstream and that the branch-lines are reflected straight and parallel to the current owing to the hydrodynamic forces.

In the side view of the system (Fig. 7, top), the values (unit: kg) nearby elements express the tension of the corresponding element. The numerical results for rope tension showed that the rope tensions diminished downstream. The decrease trend of tension was clearly observed by the tensivity of rope in the model testing.

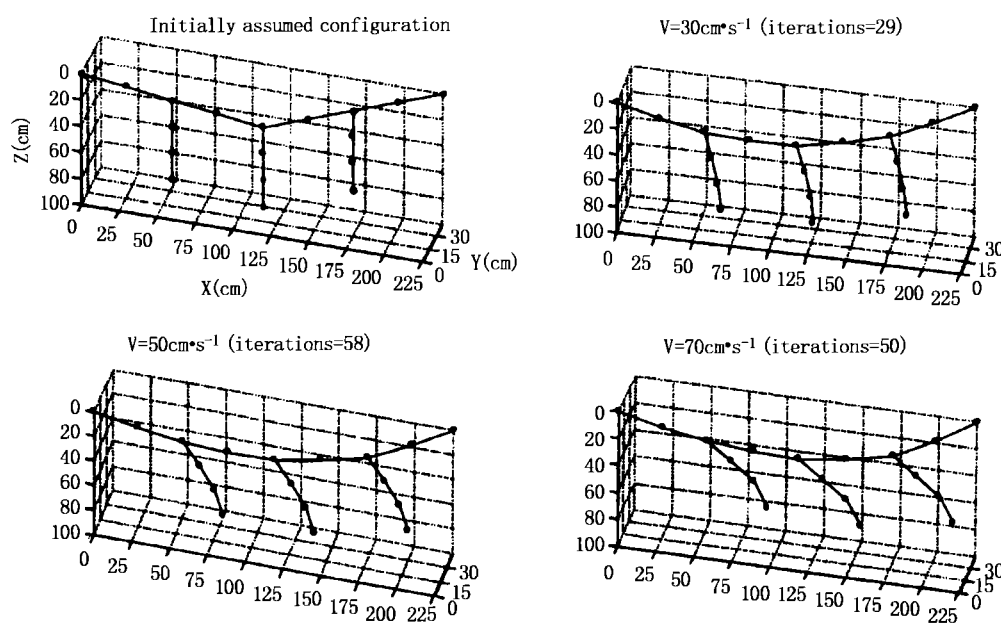


Fig. 6 Effect of current speed on the shape of the long-line model when placed at an angle of 10° relative to the current

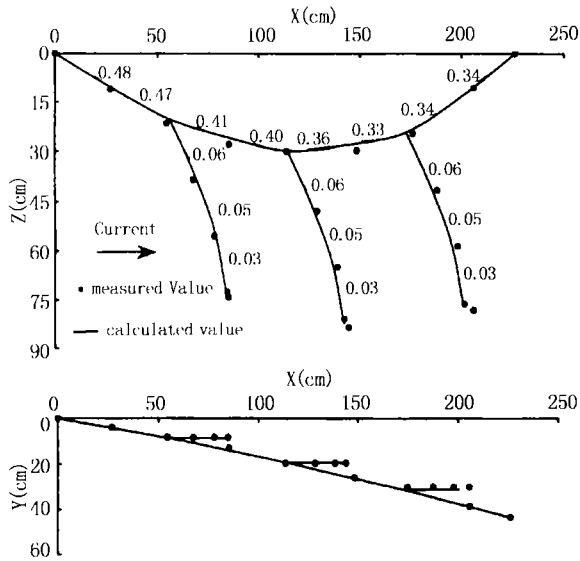


Fig.7 Comparison between the experimented values and calculated shape of the simplified long-line model in X-Z and X-Y when $\alpha = 10^\circ$ and $V = 0.7 \text{ m} \cdot \text{s}^{-1}$. The values in the figure denote the element tension(kg)

4 Discussions

(1) In the above mixed formulation, since the strain-displacement relationship can be maintained completely without any omission, the solution with desired accuracy can be ensured in the Newton-Raphson iterative procedure adopted without taking the recurrence of the load increments for any intensity of the applied load, in the sense of the problems of small strain and large displacement.

(2) In order to accurately model the shape-dependent hydrodynamic characteristics, the loading and shape iterative procedure has been employed.

(3) Iterative solution for nonlinear problems commonly requires initial values at the beginning of calculation, and the initial values provided will affect computing time. Theoretically, the closer to the correct solution the initial values are, the shorter the computation time will be. In this paper, for the sake of convenience, the computations were started from a simple assumed shape, i. e. mainline is an isosceles triangle and the branch-lines are upright, the values in brackets in Fig. 5 and Fig. 6 express the number of iteration.

(4) In commercial turfa fishery, the fishing operation status of each basic unit of the longline gear (including mainline, branch-lines and hooks between the two neighboring buoys) can be considered to be

same and the distance of the mainline can be generally regarded almost unchangeable during fishing operation. So, as mentioned above, we could only use a basic unit to approach the whole longline assuming that its two ends are fixed.

(5) Although the tension simulation results did not be compared in this paper because it is very difficult to be measured, the tension distribution pattern from Fig. 5 and Fig. 7 agrees with the experimental observation (such as the tensivity of each element in model testing) and qualitative analysis from common knowledge. So, it is shown that the simulation results of tension distribution are reliable and that the calculation results are of very important significance for correctly selecting fishing gear material to ensure the gear strength.

Because the factors affecting longline behavior during operation are very complex, such as fishing boat speed during operation and fishing ground conditions (wave, current and wind), etc., it has been considered very difficult to predict numerically the operation status of a longline for a long time^[3-7]. In this paper, we validly divided the supple rope system into so-called finite rope elements and correspondingly regarded the whole system as an assembly of such discrete elements. The results showed that the proposed method has excellent global convergence and good accuracy. The 3-D configuration and tension distribution of a longline are very difficult to be measured since it works underwater. So, we hope the proposed method can present a useful alternative numerical tool for the improvement and design of longline.

References:

- [1] 苗振清, 黄锡昌. 世界金枪鱼渔业现状分析[J]. 浙江海洋学院学报, 2002, 21(4): 307-313
- [2] 许柳雄. 中国金枪鱼渔业现状及发展空间探讨[A]. 中国水产捕捞学术研讨会论文集(四)[C]. 2001, 4: 1-6
- [3] 戴小杰, 项忆军. 热带大西洋公海金枪鱼延绳钓渔获物钩率的分析[J]. 水产学报, 2000, 24(1): 81-85
- [4] 宋利明. 中西太平洋金枪鱼延绳钓捕捞技术的改进[J]. 上海水产大学学报, 1998, 7(4): 345-347.
- [5] 叶振江, 梁振林, 邢智良, 等. 金枪鱼延绳钓不同位置钩渔获效率的研究[J]. 青岛海洋大学学报, 2001, 31(5): 707-712
- [6] 宋利明. 大西洋中部金枪鱼延绳钓捕捞技术初探[J]. 上海水产大学学报, 1997, 6(2): 139-142.
- [7] Mizuno K, Okazaki M, Okamura H. Estimation of underwater shape of tuna long-line by using micro-BTs[J]. Bull Nat Res Inst Far Seas Fish, 1997, 34: 1-24
- [8] Mizuno K, Okazaki M, Miyabe N. Fluctuation of long-line shortening rate and its effect on underwater long-line shape[J].

- Bull Nat Res Inst Far Seas Fish, 1998, 35: 155-164
- [9] Oden J T Finite element applications in nonlinear structural analysis[A] Proc of the ASCE: symposium on application of finite element methods in civil engineering[C], 1969, 419-456.
- [10] Matthies H, Strang G The solution of nonlinear finite element equations[J] International J for Numerical Methods in Engineering, 1979, 14: 1613-1626
- [11] Kawamata S, Magara E, Kunita J Analysis of cable nets in mixed formulation[A] Theory and practice in finite element structural analysis Proc of the 1973 Tokyo Seminar on Finite Element Analysis[C] Univ of Tokyo Press, 1973 157-175
- [12] Wan R Study on numerical simulation for fishing nets[D] Tokyo, Japan Tokyo Univ Fish, 2002
- [13] 王勖成, 邵敏 有限单元法基本原理和数值方法(第二版)[M] 北京: 清华大学出版社, 1997 22-35
- [14] Miyazaki Y Basic investigations on the resistance of fishing nets-V, the resistance of ropes placed obliquely to the stream[J] J Tokyo Univ Fish, 1970, 56: 49-86.

金枪鱼延绳钓捕捞作业状态的数值模拟

万 荣, 崔江浩, 宋协法, 唐衍力, 赵芬芳, 黄六一

(中国海洋大学水产学院, 山东 青岛 266003)

摘要: 一种基于有限元原理的非线性混合法被用于预测捕捞作业中的金枪鱼延绳钓的形状与张力, 为渔具设计提供理论方法, 并以期在设计阶段能替代传统的水槽模型试验, 为实际渔业生产作业调整提供有益的技术参数。构成延绳钓渔具的绳索可以被一系列绝对柔软的被称作绳索要素的单元所模拟, 因此, 整个延绳钓渔具可以被看作一系列绳索要素在其两端点通过无摩擦铰接连接而成的集合体。根据最小位能原理, 可以导出描述系统平衡状态的非线性基本平衡方程式。利用 Newton-Raphson 方法, 通过一系列的负荷-形状迭代法求解基本平衡方程式, 可以获得海流作用下延绳钓渔具作业时的形状和张力的数值解。简化模型的回流水槽试验验证表明, 本方法具有较好的计算精度和解的收敛性与稳定性。

关键词: 有限元解析; 金枪鱼; 延绳钓; 形状与张力

中图分类号: S972

文献标识码: A

收稿日期: 2003-07-14

资助项目: 山东省中青年科学家奖励基金; 教育部留学回国人员基金; 高等学校博士学科点专项科研基金资助(20040423007)

作者简介: 万 荣(1963-), 男, 浙江温岭人, 博士, 教授, 主要从事渔具力学和设施渔业工程数值模拟研究。Tel: 0532-2032375, E-mail: rongwan@ouc.edu.cn